Shock-Excited OH Maser Emission Outlining the Galactic Center Supernova Remnant G359.1-0.05

F. Yusef-Zadeh, K. I. Uchida, D. Roberts

A search using the Very Large Array was performed for 1720-megahertz OH maser line emission from a number of nonthermal radio continuum sources in the galactic center region. The 1720-megahertz transition has recently been noted for its potential as a tracer of shock activity. The most striking result was the detection of extended 1720-megahertz OH maser emission, as well as a number of compact OH maser features, along the interface between a large-scale continuum shell (G359.1-0.5) and its surrounding ring of high-velocity molecular gas. The morphological correlation among the neutral gas, the nonthermal shell, and the maser features provides strong support for the hypothesis that the 1720-megahertz maser line of OH arises from gas shocked by the impact of the expanding supernova remnant into the molecular material. However, the radial velocities of the molecular cloud surrounding G359.1-0.5 are more negative than that of the OH maser spots by more than 50 kilometers per second. Here it is suggested that only the low-radial-velocity component of the carbon monoxide material at the limb of the remnant satisfies the physical conditions required for collisional pumping of the OH 1720-megahertz line behind the expanding shock front.

The apparent association of 1720-MHz OH masers with supernovas has recently been emphasized by a high-resolution study of the supernova remnant W28, performed by Frail *et al.* (*1*). The 1720-MHz OH maser clumps are observed along the interface between the supernova remnant and an adjacent molecular cloud, leading Frail *et al.* to suggest shock activity as the pumping source of the masers. This idea is in stark contrast to 1665- and 1667-MHz OH maser clumps, which are generally observed in star-forming regions and in the circumstellar envelopes of evolved stars and are thus believed to be radiatively pumped. This result has motivated us to look in the galactic center region, where a number of nonthermal features are believed to be interacting with thermal gas and where shock activity is likely to be prevalent.

Figure 1 presents a 21-cm wavelength (λ) radio continuum image of the nonthermal shell G359.1-0.5, taken as part of an HI absorption line study by Uchida *et al.* (*2*) using the Very Large Array (VLA). The continuum shell is directly centered on the image. There is also an unusual, threadlike, nonthermal radio continuum structure, sometimes referred to as the "Snake" (*3*), crossing the western edge of the G359.1-0.5 shell. The Snake is one of several filamentary features that are found only within the inner degree of the galactic center (*4*) and that perhaps manifest a large-scale (~100 pc) poloidal magnetic field component. The HI absorption line study implies that both the shell and the filamentary feature are located at the distance of the galactic center (here assumed to be 8.5 kpc). Centered on and concentric with the radio continuum shell in Fig. 1 is a nearly continuous ring of molecular gas (*5*), displayed as contours of integrated ^{12}CO (rotation quantum number $J = 1$ to 0) emission (with velocities ranging between -60 and -190 km s^{-1}), with a mean radius of about 12′. Because of galactic rotation, gas located at the distance of the galactic center is typically observed at high radial velocities ($V =$ 50 to 250 km s^{-1}), whereas gas in the foreground or background of the galactic center is found to have velocity near 0 km s^{-1}. There are, however, a number of low-radial-velocity gas clouds moving in noncircular orbits about the galactic center (*6*). But in general, the large radial velocities of the molecular shell ($V = -190$ and -60 km s^{-1}) and its large linewidths (35 to 50 km s^{-1}) suggest that the molecular shell, like the continuum shell it surrounds, is located within the galactic center region.

The OH 1720-MHz maser line observations were made on 5 February 1995 in the direction of a number of galactic center sources, with the use of the compact DnC configuration of the VLA. Two of the six fields observed cover the G359.1-0.5 region; their phase centers are at $\alpha(1950) = 17^h\ 43^m$, $\delta(1950) = -29°55'$ and $\alpha(1950) = 17^h\ 41^m\ 30^s$, $\delta(1950) = -29°55'$, which are the eastern and western edges of the shell, respectively (α, right ascension; δ, declination). Each field was observed for about 20 min with two intermediate frequency (IF) pairs simultaneously measuring the right- and left-circular polarized emission components. Each IF had a total bandwidth of 1.5625 MHz (273 km s^{-1}) and was split among 128 channels. The IFs for a particular polarization were centered at $V = -80$ and $+80$ km s^{-1} to maximize the total velocity coverage. The data from the two IFs were combined for a total velocity coverage of ± 216 km s^{-1}, then Hanning-smoothed off-line to give a velocity resolution of 4.25 km s^{-1}. The spatial images were deconvolved with the CLEAN algorithm with the use of a clean beam 71″ × 33″ in size, oriented at a position angle of 12°. The channel and continuum root-mean-square noise are about 4 and 20 millijansky (mJy) per beam, respectively. The two fields were corrected for the primary beam attenuation and were linearly added after being weighted by the inverse of the variance.

Figure 2 shows an OH line emission image, integrated between the velocities of -13.6 and -0.8 km s^{-1}, produced by combining the two IF's and making a mosaic of the overlapping fields. Superimposed on OH contours is the continuum grayscale image of the G359.1-0.5 supernova remnant (SNR). This figure illustrates a striking correlation between the OH spots and the edge of the nonthermal remnant. The Gaussian-fitted positions of the six distinct compact OH emission spots (sources A through E), as well as their surface brightnesses and velocities, are listed in Table 1. All of the features have narrow linewidths that are either equivalent to or less than that of a single unsmoothed channel [$\Delta V_{FWHM} = 2.125$ km s^{-1} (FWHM, full width at half maximum)] and all are generally found peaking at the velocity of ≈ -5 km s^{-1}. All of the OH sources reported here are observed in both of the original overlapping fields and in each of the IFs, thus eliminating any possibility that they are spurious observations.

Figure 3 is a close-up view of the region where the Snake crosses the G359.1-0.5 shell; it is also the location of the brightest compact OH maser spot (source A), of the brightest continuum emission, and of an extended OH component. Contours of the OH 1720-MHz line emission are superimposed on the color radio continuum image. The elongated OH feature is resolved spatially in the direction along the limb-brightened edge of the remnant; it extends from source A for about 5′, following the edge of the remnant. The extended component has velocities ranging between -11 and -3 km s^{-1} and peaks in surface brightness (20 mJy per beam) at -8 km s^{-1}. Figure 4, which shows a spectrum of source A, indicates a peak flux density of 760 mJy per beam [at $V_{LSR} = -4.47$ km s^{-1} (LSR, local standard of rest)]. Because this exper-

F. Yusef-Zadeh, Department of Physics and Astronomy, Northwestern University, 2145 North Sheridan Road, Evanston, IL 60208, USA.
K. I. Uchida, Max Planck Institut für Radioastronomie, auf dem Hügel 69, 53121 Bonn, Germany.
D. Roberts, Department of Astronomy, University of Illinois at Urbana, Champaign, IL 61801, USA.

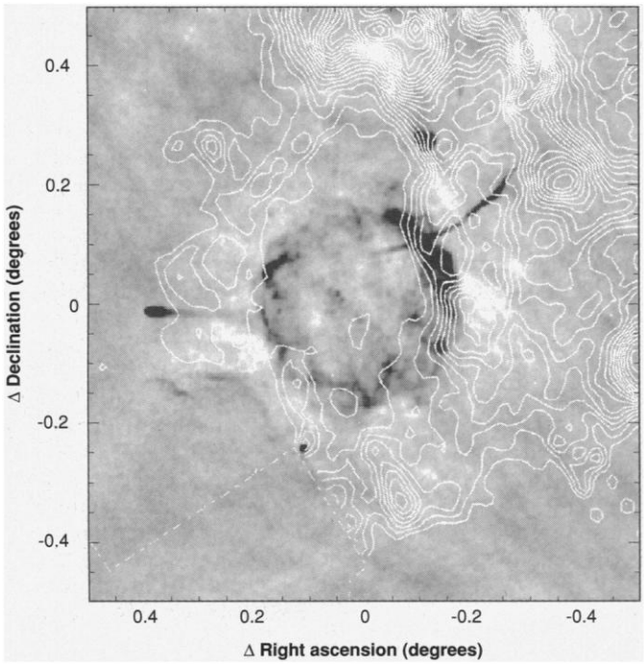

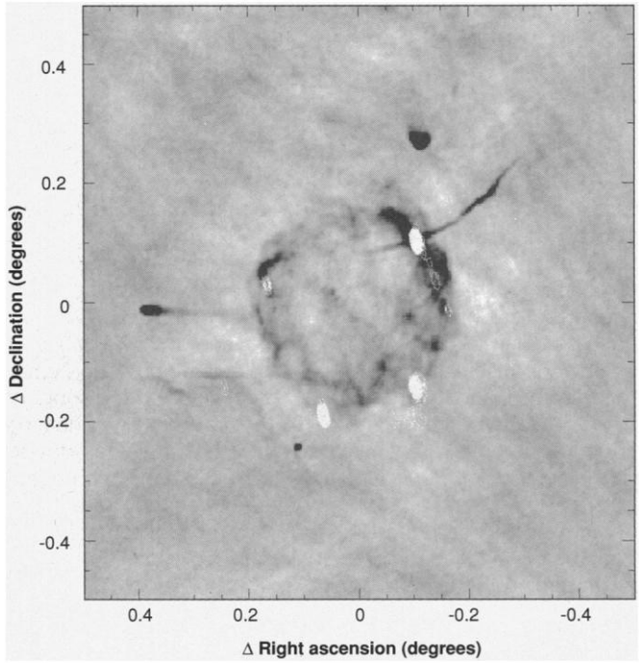

Fig. 1 (left). Radiograph of the λ 21-cm continuum emission from G359.1-0.5 with a spatial resolution of 32.6″ × 30.8″ (position angle = 56°). Dotted lines indicate the border of the CO map. The long narrow magnetic structure known as the Snake crosses the western side of the remnant. Contours of integrated ^{12}CO line intensity between −190 and −60 km s^{-1} are superimposed on the radiograph. The contour levels are set at 75 K km^{-1} s^{-1} and increase in increments of 30 K km^{-1} s^{-1} up to 800 K km ^{1} s ^{1}. The reference position (0, 0) corresponds to α (1950) = $17^h 42^m 15^s$, δ (1950) = −29°56′. **Fig. 2 (right).** The distribution of the OH 1720-MHz maser features, integrated between the velocities of −13.6 and −0.8 km s^{-1}, are presented as contours and are superimposed on the radio continuum image shown in Fig. 1.

iment was designed to detect compact sources, the presence of an extended structure in the image came as a surprise. It is possible that there are more weak and extended OH line-emitting features surrounding the remnant but that they have been suppressed or "resolved out" due to a lack of complete *uv* coverage. It is also possible that many of the OH features will break up into a number of compact sources if observations are made at higher spatial and spectral resolutions. Thermal OH 1720-MHz emission is unlikely to explain the narrow linewidths of the OH features, because galactic center molecular clouds are known to have large internal velocity dispersions (30 to 50 km s^{-1}) (6). Thus, we assert that the 1720-MHz emission features are nonthermal in nature.

Are the OH masers physically associated with the G359.1-0.5 SNR? One argument in favor of the association is the remarkable spatial correlation of OH features with the limb of the nonthermal shell, which is itself thought to be interacting with a surrounding ring of neutral gas (5). This picture is similar to that of the W28 region, where numerous distinct OH 1720-MHz maser spots are found along the interface between the nonthermal shell and an adjacent molecular cloud. It has been argued that the W28 maser spots are pumped collisionally behind the shock where H_2 molecules with kinetic temperatures below 200 K cause a population inversion in the OH molecules. The OH 1720-MHz line emission seen toward the SNR W28, with an observed expansion velocity of 50 to 80 km s^{-1}, would imply a J-type shock (*1*). Conspicuously absent from this region are any 1665- and 1667-MHz OH maser emissions, which are believed to be the result of radiative pumping.

It should also be noted that source A, which is the brightest of the compact OH sources, is situated at the very location where the Snake intersects the G359.1-0.5 continuum shell (Fig. 3). This is particularly relevant to the suggestion made by some that the filamentary Snake is associated with the supernova shell. In the λ 21-cm continuum image, the brightest segment of the nonthermal shell is centered around the point of intersection with the Snake. The spectral index of this segment of G359.1-0.5 (where the Snake crosses) is flatter than that of the rest of G359.1-0.5 (*3*), perhaps suggesting the deposition of energy from the filament into the shell at this location. In addition, the ^{12}CO and OH emissions appear to be strongest on the side of the nonthermal shell where the Snake is found. The existence of an 1720-MHz OH maser spot exactly where the Snake and the shell intersect is consistent with the assertion that they are associated and interacting.

One puzzling point, however, is the striking contrast between the observed radial velocities of the OH spots (~−5 km s^{-1}) and those of the CO ring (V = −100 km s^{-1}). A potential solution to this problem would have the OH gas contained in dark clouds that are foreground to the galactic center (thus having small radial velocities), amplifying the background radiation along the limb of the remnant. In this

Table 1. Parameters of the OH masers in G359.1-0.5.

OH maser source	α (1950)	δ (1950)	V_{LSR} (km s^{-1})	Flux density (mJy)
A	17 41 46.042	−29 49 51.03	−4.47	761
B	17 41 29.836	−29 56 46.63	−2.95	59.5
C1	17 41 43.867	−30 04 47.95	−3.19	215
C2	17 41 45.791	−30 04 35.17	−5.57	732
D	17 42 32.445	−30 04 24.11	−5.28	639
E	17 43 0.824	−29 54 11.72	−5.08	93

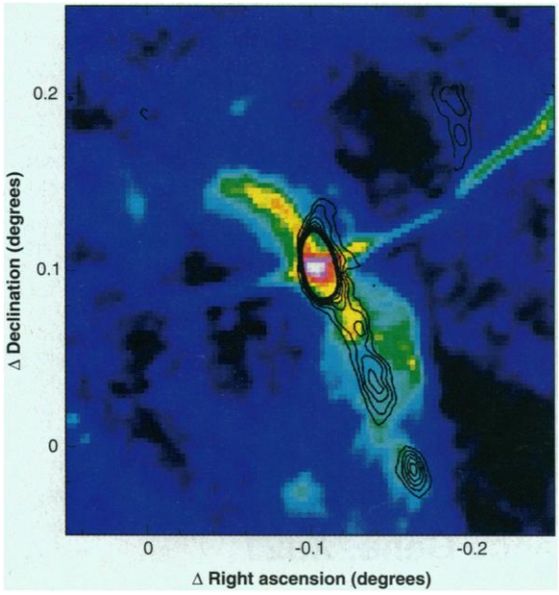

Fig. 3. The region where the Snake and G359.1-0.5 cross each other coincides with the brightest detected maser feature (source A) and the brightest continuum emission. The extended maser feature source, though weak in comparison with compact sources, appears to link sources A and B. The contour levels start at 25 mJy per beam × km s^{-1} and increase in increments of 50 mJy per beam × km s^{-1}. The contours seen in the upper right corner of the image are artifacts due to the primary beam correction.

scenario, the maser clumps are not associated physically with the G359.1-0.5 nonthermal shell or its surrounding ring of high-velocity (and thus, galactic center) gas. A similar interpretation attributes a number of 1720-MHz emission spots to clouds located along the spiral arms of the galaxy (*7*), stimulated by strong background continuum sources. There are a number of reasons, however, why we believe it unlikely that the emission arises from OH gas foreground to the G359.1-0.5 SNR. One is the fact that two of the maser sources (B and D) are in portions of the remnant where no continuum emission is detected above 5 mJy. Another is that no masers are observed along the portion of the bright Snake that extends beyond the perimeter of the shell or toward some of the bright portions of the shell itself interior to its edge. This is contrary to the situation in which the background radiation is responsible for stimulating the maser spots. The only alternative is a contrived scenario in which very clumpy foreground material is distributed in a ring coincident with the limb of the continuum shell, thus avoiding the center of the remnant and the Snake.

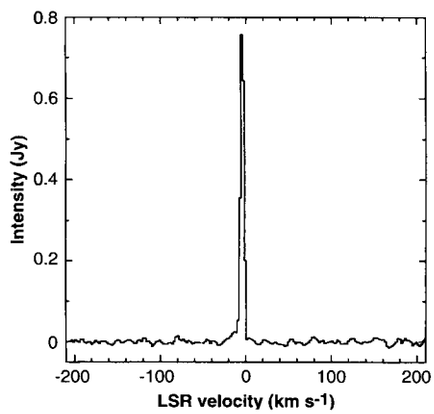

Fig. 4. A typical spectrum of the OH 1720-MHz emission from source A. The background continuum emission at this position is about 150 mJy per beam.

Another hypothesis that accounts for the low velocities of the OH maser spots is that they are physically associated with the expanding forefront of the SNR, but the supernova remnant itself is located outside of the galactic center region. However, this scenario also has a number of serious drawbacks. The idea that the supernova remnant is outside of the galactic center is contrary to the position indicated by a previous λ 21-cm HI absorption line study (*2*). Moreover, the SNR would need to be located beyond the galactic center, making it unusually large in physical size. The ROSAT satellite did not detect x-rays from the supernova remnant, as would be expected if it were a local source (that is, foreground to the galactic center). It also follows from this scenario that the SNR is not associated with high-velocity ring of CO gas which, because of its high velocities and large linewidths, is almost assuredly located in the galactic center region. The association of the SNR, its surrounding ring of CO molecular gas, and the intersecting Snake is then relegated simply to a remarkable coincidence.

The OH 1720-MHz masers observed along the interfaces of the SNR and molecular clouds are uncommon and appear to be different from OH emission features seen along the spiral arms (*7*) (which have nonmaser characteristics). A fact that may support the assertion that shocks are involved is that most of the maser sources, including the extended OH feature, are found along the western edge (in galactic coordinates) of the remnant. At this location, the nonthermal emission from the shell is stronger and the CO molecular gas is obviously more prevalent (see Fig. 1). There is only one observed maser spot (source E) along the eastern edge of the remnant where the CO velocities are about 100 km s^{-1} more negative than those of the western side of the SNR and thus far less consistent with the low velocity of the maser spot itself (a few kilometers per second).

In general, the seemingly different kinematics of the CO gas and OH emission spots may be reconciled, given the large linewidth of the H_2 gas and with the assumption that only the low-velocity component of the colliding cloud is effective in producing the OH emission behind the shock front. In this picture, there is only a small range of densities and temperatures at which OH can be collisionally pumped and can subsequently mase ($<2.5 \times 10^4$ cm^{-3} and 15 to 200 K). According to the model presented in (*9*), preshock densities and temperatures of the molecular gas outside this range suppress maser activity. There are, potentially, some amounts of low-radial-velocity CO gas associated with the G359.1-0.5 SNR, but it is difficult to determine the distribution because of substantial contamination of the field by low-velocity foreground gas. It is not unusual to find low-radial-velocity forbidden molecular gas in the galactic center region, because large departures from circular motion and motion along inclined orbits have been evident throughout this region (*6*). Other factors might account for the low radial velocities of the OH spots. A shock front, moving obliquely with respect to the ambient magnetic field, can be responsible for redirecting the radial velocity component of the preshocked gas along the observer's transverse direction. In this scenario, the change from the radial to the transverse velocity across an oblique shock is estimated to be equal to the value of the preshocked Alfve'n velocity (*8*). As the shock front is viewed edge on, the velocity gradient is expected to be minimized along the line of sight, thus enhancing the gain of the OH 1720-MHz emission from that direction (*9*). Another geometric factor that can be attributed to the enhancement of the gain toward the low-radial-velocity maser spots is that the gain is maximized along the path length toward the limb of the remnant where the largest component of the velocity of the gas is tangential to the observer's line of sight.

The 100 km s^{-1} velocity difference across the CO shell has been suggested to be the result of shear due to differential galactic rotation (*5*), a factor especially important for objects located near the galactic center. The constant velocity of OH masers across the remnant suggests that

the OH features have not yet participated in the general shear motion of the gas cloud surrounding the remnant. In this scenario, the OH spots are the sites where the gas has most recently been shocked to form masers. The time scale for the shear to be effective is about 5×10^5 years, which is much larger than the typical lifetime of maser clouds.

The distribution of 1720-MHz OH masers along the SNR–CO-cloud interface suggests that there is an association between the three components and that the OH masers are being generated behind a shock. However, questions regarding the striking kinematic differences between the OH and CO gas need to be addressed in more detail. Future observations of CS to search for low-velocity molecular gas associated with the G359.1-0.5 SNR, as well as a search for the 1665- and 1667-MHz OH lines, are needed to confirm the nature of the OH 1720-MHz maser pumping mechanism and the nature of the association between the nonthermal remnant and its surrounding ring of molecular gas.

REFERENCES AND NOTES

1. D. A. Frail, W. M. Goss, V. I. Slysh, *Astrophys. J.* **424**, L111 (1994).
2. K. I. Uchida, M. Morris, M. Yusef-Zadeh, *Astron. J.* **104**, 1533 (1992).
3. A. D. Gray, L. E. Cram, R. D. Ekers, W. M. Goss, *Nature* **353**, 237 (1991).
4. F. Yusef-Zadeh, M. Morris, D. Chance, *ibid.* **310**, 557 (1984); H. Liszt, *Astrophys. J.* **293**, L65 (1985).
5. K. I. Uchida, M. Morris, J. Bally, M. Pound, F. Yusef-Zadeh, *Astrophys. J.* **398**, 128 (1992).
6. J. Bally, A. A. Stark, R. W. Wilson, C. Henkel, *ibid.* **324**, 223 (1988).
7. B. E. Turner, *ibid.* **255**, L33 (1982).
8. D. Hollenbach, and C. F. McKee, *ibid.* **342**, 306 (1989); M. Wardle, *Mon. Not. R. Astron. Soc.* **251**, 119 (1991).
9. M. Elitzur, *Astrophys. J.* **203**, 124 (1976).

10. We thank B. Purcell and M. Wardle for useful discussions. D.R. acknowledges support from the Laboratory for Astronomical Imaging at the University of Illinois. F.Y. was supported by NASA grant NAGW-2518.

19 July 1995; accepted 28 September 1995

A Receptor Kinase–Like Protein Encoded by the Rice Disease Resistance Gene, *Xa21*

Wen-Yuan Song,* Guo-Liang Wang,* Li-Li Chen, Han-Suk Kim, Li-Ya Pi, Tom Holsten, J. Gardner, Bei Wang,† Wen-Xue Zhai, Li-Huang Zhu, Claude Fauquet, Pamela Ronald‡

The rice *Xa21* gene, which confers resistance to *Xanthomonas oryzae* pv. *oryzae* race 6, was isolated by positional cloning. Fifty transgenic rice plants carrying the cloned *Xa21* gene display high levels of resistance to the pathogen. The sequence of the predicted protein, which carries both a leucine-rich repeat motif and a serine-threonine kinase–like domain, suggests a role in cell surface recognition of a pathogen ligand and subsequent activation of an intracellular defense response. Characterization of *Xa21* should facilitate understanding of plant disease resistance and lead to engineered resistance in rice.

Receptor protein kinases mediate cellular signaling processes in diverse biological systems. In many animal systems, the binding of ligands to the extracellular receptor domain of these proteins activates a cytoplasmic tyrosine kinase domain. This interaction produces a variety of cellular responses, such as cell proliferation, differentiation, and survival (*1*). The few plant receptor kinase–like proteins that have been studied to date carry serine-threonine specificity in the kinase domain (*2*). One of these proteins, the S-receptor kinase (SRK), has been postulated to mediate self-recognition between pollen and stigma during pollination, although transformation experiments have not yet conclusively demonstrated such a role (*3*). The biological function of the other plant receptor kinase–like proteins remains unclear.

One possible role for these proteins in plants is in mediating disease resistance. Cellular signaling processes appear to be of central importance to the mechanisms by which plants resist viral, bacterial, and fungal pathogens. Evidence for this model comes from the recent characterization of several disease resistance genes from dicotyledonous species. The deduced amino acid sequence of five of these genes demonstrates the presence of either a serine-threonine kinase (STK) or a leucine-rich repeat (LRR) domain, suggesting a role in protein phosphorylation or protein-protein interactions (*4*).

Three members of the monocotyledonous family Poaceae (maize, rice, and wheat) provide most of the calories consumed by humans. Despite their agronomic importance, molecular genetic studies of monocots have been hindered by the large genome size of most of these plants. Rice provides an amenable system for positional cloning in monocots because of its small genome size, extensive genetic map, and ease of transformation.

Here we report positional cloning of the rice gene *Xa21*, which confers resistance against the bacterial pathogen *Xanthomonas oryzae* pv. *oryzae* race 6 (*Xoo*) (*5*). The de-

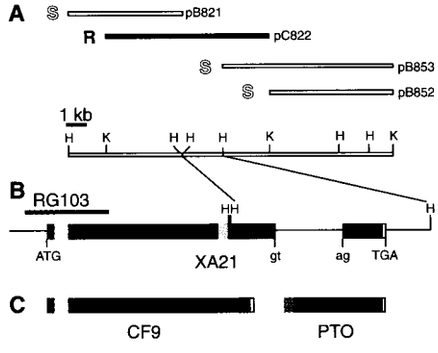

Fig. 1. (**A**) Partial restriction enzyme map and rice complementation analysis of cosmid 116. Transformation of Taipei 309 with genomic subclones pB821, pC822, pB852, and pB853 produced plants with resistance (R) or susceptibility (S) to *Xoo* race 6 strain PX099Az. The 9.6-kb Kpn I DNA fragment of cosmid 116 was cloned into plasmid pTA818 (*6*) to generate pC822. Hind III (H), Kpn I (K), and Hind III–Kpn I DNA fragments of cosmid 116 were ligated to pBluescript SK$^+$ (Stratagene) to generate pB821, pB852, and pB853, respectively. Scale is indicated by a bar. (**B**) The XA21-coding region and deduced amino acid sequence. The ATG and TGA codons, the RG103-hybridizing region, and 5′ and 3′ splice junctions corresponding to the consensus sequences of eukaryotic mRNAs are marked. The intron is designated by a horizontal bar. (**C**) The tomato CF9 and PTO deduced amino acid sequences. Domains of the protein are indicated in (B) and (C) as follows: blue, presumed signal peptide; yellow, unknown; red, LRR; black, transmembrane; pink, juxtamembrane; green, kinase; turquoise, nonhomologous region; and white, COOH-terminal tail.

W.-Y. Song, G.-L. Wang, L.-Y. Pi, T. Holsten, B. Wang, P. Ronald, Department of Plant Pathology, University of California, Davis, CA 95616, USA.
L.-L. Chen and C. Fauquet, International Laboratory for Tropical Agricultural Biotechnology/The Scripps Research Institute–Institut Francais de Recherche Scientifique et Technique pour le Developpement en Cooperation (ORSTOM), Scripps Institute, Plant Division MRC7, 10666 North Torrey Pines Road, La Jolla, CA 92037, USA.
H.-S. Kim and J. Gardner, Center for Engineering Plants for Resistance Against Pathogens, University of California, Davis, CA 95616, USA.
W.-X. Zhai and L.-H. Zhu, Institute of Genetics, Academic Sinica, Beijing, China 100101.

*These authors contributed equally to this work.
†Present address: Department of Molecular Microbiology, School of Medicine, Washington University, St. Louis, MO 63110, USA.
‡To whom correspondence should be addressed.